GYROLESS ATTITUDE AND RATE ESTIMATION ALGORITHMS FOR THE FUSE SPACECRAFT

Rick Harman*, **Julie Thienel**† **and Yaakov Oshman**‡

This paper documents the testing and development of magnetometer-based gyroless attitude and rate estimation algorithms for the Far Ultraviolet Spectroscopic Explorer (FUSE). The results of two approaches are presented, one relies on a kinematic model for propagation, a method used in aircraft tracking, and the other is a pseudo-linear Kalman filter that utilizes Euler's equations in the propagation of the estimated rate. Both algorithms are tested using flight data collected over a few months after the failure of two of the reaction wheels. The question of closed-loop stability is addressed. The ability of the controller to meet the science slew requirements, without the gyros, is analyzed.

INTRODUCTION

The Far Ultraviolet Spectroscopic Explorer (FUSE) is equipped with two ring laser gyros on each of the spacecraft body axes. In May 2001 one gyro failed. In July 2003 a second gyro failed. It is anticipated that all of the remaining gyros will fail, based on intensity warnings. In addition to the gyro failure, two of four reaction wheels failed in late 2001. The spacecraft control now relies heavily on magnetic torque to perform the necessary science maneuvers and hold on target. The only sensor consistently available during slews is a magnetometer. Thus, this work focuses on the development and testing of attitude and angular rate estimation algorithms using magnetometer only data for the FUSE satellite.

Estimating the attitude at a given time point requires at least two vector measurements. With only one vector measurement, attitude estimation is possible with a recursive algorithm and a vector that changes direction over time. Since the magnetic field vector changes direction, it is suitable for a single sensor estimation algorithm. However, the attitude estimate must be propagated from one time to the next with an estimate of the spacecraft rate. Typically the rate is supplied by a gyro. Without a gyro, an estimate of the rate must be provided by some other means.

*Aerospace Engineer, Flight Dynamics Analysis Branch, NASA Goddard Space Flight Center, (301) 286-5125, (301) 286-0369 (FAX), email: richard.r.harman@nasa.gov

†NASA Goddard Space Flight Center, Flight Dynamics Analysis Branch, Greenbelt, MD 20771, phone: 301-286-9033, fax: 301-286-0369, email: julie.thienel@nasa.gov

‡Technion—Israel Institute of Technology, Department of Aerospace Engineering and Asher Space Research Institute, Haifa 32000, Israel, phone/fax: +972-4-829-3803, email: Yaakov.Oshman@technion.ac.il

Gyros are notorious, even those of the highest grade, for their low reliability. A case in point is provided by the Hubble space telescope (HST), which was put on safe hold mode on November 13, 1999 after four of its six world class gyros failed.[1] This fact, as well as known cases of satellite thrusters anomalies, which often result in tumbling situations (during which the gyros are saturated by the high spacecraft (SC) angular rates), have motivated the need for the development of alternative rate estimation algorithms.

Several methods have been introduced in the past for angular rate estimation of gyroless SC. Some of these estimate the body angular rates within an attitude/attitude rates estimator, where the measurements are the three components of a body referenced vector, employing deterministic algorithms or filtering techniques. Most methods use the spacecraft dynamic model, i.e., Euler's equation of motion. Thus, Ref. 2 develops an extended Kalman filter (EKF) for the estimation of SC attitude and angular rate from three-axis magnetometer (TAM) readings. Assuming that the SC ephemeris is well known, the method is based on a known model for the Earth's magnetic field, takes about an orbit to converge, and yields only coarse accuracy (making it suitable only for emergency modes). Challa and Natanson[3] combined a deterministic algorithm and an extended Kalman filter algorithm to estimate attitude and a correction to the estimated rate, using magnetometer data. They modeled the correction term as a first-order Markov model. The corrected rate estimate is propagated with Euler's equation. No a priori information about the state is required, as the deterministic algorithm provides the a priori state for the filter.

In other methods,[4–7] SC angular rate components are estimated separately, using either deterministic or filtering based algorithms, but always making use of independently known attitude information. The method presented in Ref. 4 is based on an extension of the suboptimal interlaced Kalman filter scheme proposed in Ref. 8 and is able to estimate the angular rates from two measured directional vectors, or from a single vector for the relatively short duration of eclipses. In Ref. 5 two estimation methods are presented, based on the ability to decompose the SC dynamics – namely, Euler's equations including internal torque – into the product of an angular rate dependent matrix and the angular vector itself. In Ref. 6 a connection is established among various methods, available in the literature, that are aimed at estimating the SC angular rates. It is shown how the so-called derivative approach, where the attitude, in an arbitrary parameterization, is differentiated to relate it to the satellite angular rate, and the estimation approach, where the raw measurements are fed directly into a filter, are both based on an equation relating the attitude, its time derivative and the angular rate. In Ref. 7 the quaternion is used for attitude representation, and two SC angular rate estimation methods are proposed. The first uses differentiated quaternion measurements to algebraically extract a noisy estimate of the angular rate vector, which is successively fed into two filters similar to those presented in Ref. 5. In the second, the raw attitude quaternion is fed directly into the filters, whose state vector is augmented to comprise the three angular rate components.

A new class of attitude rate estimation algorithms has recently been introduced in Refs. 9–11. Reference 10, which applies the general approach of Ref. 9 to the special case of Geomagnetic field measurements, assumes no attitude knowledge and uses sequential readings of the Geomagnetic field direction only, assuming that this attitude reference vector is fixed in inertial space. This renders its estimators completely independent of the SC position, and allows their operation without the mechanization of a complicated spherical

harmonics model of the Earth's magnetic field. Thus, these algorithms are geared towards applications such as de-tumbling, nutation damping, and momentum management without using rate gyroscopes. Two algorithms are presented in Ref. 10, a coarse, single-frame deterministic batch estimator, and a high-accuracy EKF. While the deterministic batch estimator is less accurate, it nevertheless cannot diverge and its output can be used to initialize the more sensitive EKF so as to avoid the latter algorithm's divergence. Motivated by Ref. 10, Ref. 11 introduces improved versions of both algorithms presented in Ref. 10. Thus, the deterministic algorithm of Ref. 11 uses a global nonlinear least-squares solver to determine the unknown angular momentum component along the magnetic field direction, while the EKF is formulated to explicitly account for the normalization constraint on the measured magnetic field direction vector, and estimates, in addition to the attitude rate vector, also corrections to 5 of the 6 inertia matrix elements, and 2 error states of the measured magnetic field direction. It should be noted that the methods of Refs. 9–11 are all model-based, that is, they use the SC Euler's equation of motion and, thus, are somewhat sensitive to the SC model's accuracy.

Two methods are examined in this work as candidates for the task of simultaneously estimating FUSE's attitude and angular rate from TAM only measurements. The first algorithm considered is based on the integrated-rate parameters (IRP) approach.[12,13] This algorithm uses a kinematic approach to the spacecraft rate modeling, much like is done in aircraft tracking. This approach is less sensitive to uncertainties in the spacecraft dynamics. This approach met both the attitude and rate knowledge requirement during the inertial periods. However, the IRP filter performed poorly during slew maneuvers. The second algorithm considered is the pseudo-linear rate estimation algorithm.[14] This algorithm combines an EKF algorithm with Euler's equations to model the spacecraft dynamics in a pseudo-linear approach. This approach requires the spacecraft actuator data from the reaction wheels and magnetic torque bars. Due to problems with this data during inertial periods, this filter did not adequately estimate the attitude.

The two algorithms are combined to form a hybrid IRP-Euler filter approach. The IRP filter is used during inertial periods. During maneuvers, the kinematics model of the IRP filter is replaced with the dynamics model based on Euler's equations. Modeling the movement of the solar arrays during a maneuver improved the dynamics model used in the pseudo-linear algorithm, resulting in a dramatic decrease in the propagation errors. The hybrid algorithm successfully provided the required attitude and rate knowledge during the inertial periods and closely followed the maneuvers.

Tests of the hybrid IRP-Euler filter approach, with a variety of data sets, are provided. Fortunately for our analysis, the FUSE project was able to provide a copious amount of flight data. The estimated attitudes are compared to the onboard attitude estimate which is an extended Kalman filter using the science star tracker and the ring laser gyros. The estimated rates are compared to the ring laser gyro output, compensated for gyro bias errors. During a maneuver, the science star tracker is not used. The gyro data provides the necessary accuracy for the onboard algorithm during the maneuver. The attitude and rate error accuracy requirements are 2 degrees and 20 arc-sec/sec, respectively, except during the maneuver period. Operating within these requirements allows the science star tracker to identify and track stars following a slew maneuver. Once the star tracker identifies stars, the attitude and rate estimates are provided by the star tracker (the star tracker estimates

a quaternion which is numerically differentiated to provide the rate). The rate estimates provided by the star tracker are comparable in accuracy to the gyro data, provided the spacecraft rates are maintained within the rate requirement.

Finally, the algorithm is required to work with a controller. This is the most challenging requirement. A closed loop simulation is developed with the hybrid IRP-Euler filter providing the state estimates for a quaternion feedback controller.[15] The truth model consists of integrating Euler's equation as well as the quaternion kinematic equation. The magnetometer is modeled as the true field in body coordinates plus white noise. As might be expected, the controller's performance is highly dependent on the accuracy of the estimator and the estimator's accuracy is highly dependent on the dynamics of the spacecraft induced by the controller. The remainder of the paper is devoted to summaries of the estimation algorithms, the controller simulation, and test results.

IRP ALGORITHM SUMMARY

The IRP algorithm is a sequential filter for estimating both the spacecraft attitude and rate from vector measurements, avoiding the use of the uncertain spacecraft dynamics model. The algorithm is only briefly summarized herein. A detailed description can be found in Ref. 12.

The attitude matrix evolves using an integrated rate parameters method. The attitude matrix differential equation is given as

$$\dot{D}(t) = \Omega(t)D(t) \tag{1}$$

where $D(t)$ is the spacecraft attitude matrix. $\Omega(t) = -[\boldsymbol{\omega}(t)\times]$, with $\boldsymbol{\omega}(t)$ the spacecraft angular velocity and $[\boldsymbol{\omega}(t)\times]$ defined as the cross product matrix

$$[\boldsymbol{\omega}(t)\times] \triangleq \begin{bmatrix} 0 & -\omega_z & \omega_y \\ \omega_z & 0 & -\omega_x \\ -\omega_y & \omega_x & 0 \end{bmatrix} \tag{2}$$

Expressing the attitude in terms of the integrated rate parameters, leads to a discrete-time version of the attitude matrix evolution given by Eq. (1), written compactly as[12]

$$D(k+1) = D[\boldsymbol{\theta}(k+1) - \boldsymbol{\theta}(k), \omega(k+1), \dot{\omega}(k+1), D(k)] \tag{3}$$

where the integrated rate parameter vector at time k is

$$\boldsymbol{\theta}(k) = [\theta_1(k)\ \theta_2(k)\ \theta_3(k)]^T \tag{4}$$

and

$$\theta_i(k) \triangleq \int_{t_0}^{t_k} \omega_i(\tau)d\tau \tag{5}$$

where $\omega_i = \omega_x, \omega_y, \omega_z$ for $i = 1, 2, 3$, respectively.

The IRP algorithm models the spacecraft angular acceleration as a zero-mean stochastic process with an exponential autocorrelation function, rather than relying on the nonlinear spacecraft dynamics model given by Euler's equation. The first-order Markov process is

$$\ddot{\boldsymbol{\omega}}(t) = -\Lambda\dot{\boldsymbol{\omega}}(t) + \tilde{\nu}(t) \tag{6}$$

where Λ is a diagonal matrix containing the acceleration decorrelation times. The driving noise, $\tilde{\nu}(t)$, is a zero-mean white process with power spectral density matrix $\tilde{Q}(t)$.[12]

Finally, the state vector in the IRP algorithm is given as

$$\boldsymbol{x}(t) = [\boldsymbol{\theta}(t)^T\ \boldsymbol{\omega}(t)^T\ \dot{\boldsymbol{\omega}}(t)^T]^T \tag{7}$$

The discrete time state equation is

$$\boldsymbol{x}(k+1) = \Phi(T)\boldsymbol{x}(k) + \boldsymbol{\nu}(k)$$

where $\boldsymbol{\nu}(k)$ is a zero-mean, white noise sequence, with covariance matrix $Q(k)$.[12] For a sampling interval, T, the state transition matrix for the discrete-time state equation is

$$\Phi(T) = \begin{bmatrix} I & TI & \Lambda^{-2}(\mathrm{e}^{-\Lambda T} - I + T\Lambda) \\ 0 & I & \Lambda^{-1}(I - \mathrm{e}^{-\Lambda T}) \\ 0 & 0 & \mathrm{e}^{-\Lambda T} \end{bmatrix} \tag{8}$$

Explicit expressions for the entries of the covariance matrix $Q(k)$ appear in Ref. 12.

Vector Measurement and Algorithm Update

The magnetometer vector measurement, in spacecraft body coordinates, is related to the true magnetic field vector as

$$\boldsymbol{b}(k+1) = D(k+1)\boldsymbol{r}(k+1) + \boldsymbol{n}_b(k+1) \tag{9}$$

where $\boldsymbol{n}_b(k+1)$ is a white sensor measurement noise, $\boldsymbol{b}(k+1)$ and $\boldsymbol{r}(k+1)$ are the magnetic field vectors in body and reference coordinates, respectively. The reference field is generated with a 10th order International Geomagnetic Reference Field model.[16]

Expanding Eq. (9) about the predicted state estimate results in the following relationship

$$\boldsymbol{b}(k+1) - \hat{D}(k+1|k)\boldsymbol{r}(k+1) = H(k+1)\delta\boldsymbol{x}(k+1) + \boldsymbol{n}_b(k+1) \tag{10}$$

where $\hat{D}(k+1|k)$ is the estimated attitude at time, k, propagated to time, $k+1$ and $H(k+1)$ is the observation matrix.[12] The error term $\delta\boldsymbol{x}(k+1)$ is defined as

$$\delta\boldsymbol{x}(k+1) = \boldsymbol{x}(k+1) - \hat{\boldsymbol{x}}(k+1 \mid k) \tag{11}$$

where $\hat{\boldsymbol{x}}(k+1 \mid k)$ is the predicted state estimate at time $k+1$ based on measurements up to time k. The state is then updated in the usual extended Kalman filter approach

$$\hat{\boldsymbol{x}}(k+1|k+1) = \hat{\boldsymbol{x}}(k+1|k) + K(k+1)(\boldsymbol{b}(k+1) - \hat{D}(k+1|k)\boldsymbol{r}(k+1)) \tag{12}$$

The gain matrix $K(k+1)$ is computed according to

$$K(k+1) = P(k+1|k)H^T(k+1)[H(k+1)P(k+1|k)H^T(k+1) + R]^{-1} \tag{13}$$

where $P(k+1|k)$ is the propagated covariance matrix and R is the covariance matrix of the white sensor measurement noise and is assumed to be constant. The covariance matrix is updated according to

$$\begin{aligned} P(k+1|k+1) = [I - K(k+1)H(k+1)]P(k+1|k)[I - K(k+1)H(k+1)]^T \\ + K(k+1)RK(k+1)^T \end{aligned} \tag{14}$$

Following the state update, the attitude matrix is updated with the integrated rate parameters, the state is adjusted for a reset of the integrated rate parameters (since they are completely incorporated into the attitude matrix), and then the attitude matrix is normalized.[12]

IRP Prediction

The state is propagated forward with

$$\boldsymbol{x}(k+1 \mid k) = \Phi(T)\hat{\boldsymbol{x}}^c(k \mid k) \tag{15}$$

where $\Phi(T)$ is given in Eq. (8), and $\hat{\boldsymbol{x}}^c(k \mid k)$ is the state update after reset. The covariance is propagated according

$$P(k+1 \mid k) = \Phi(T)P(k \mid k)\Phi(t)^T + Q(k) \tag{16}$$

The attitude matrix is propagated forward as a function of the propagated state and the current, orthogonalized attitude matrix.[12]

PSEUDO-LINEAR DYNAMICS MODEL

The IRP algorithm provided estimates of the attitude and rate within the FUSE requirements during the inertial periods. During the maneuvers, the rate estimates did not follow the gyro data adequately. In an attempt to improve the rate estimate during a maneuver, the IRP rate propagation was augmented with a pseudo-linear version of Euler's equation.[14]

The dynamics equation of a rigid spacecraft is given, in general, as

$$\frac{d}{dt}(I(t)\boldsymbol{\omega}(t) + \boldsymbol{h}(t)) = T(t)$$

$$\dot{I}(t)\boldsymbol{\omega}(t) + I(t)\dot{\boldsymbol{\omega}}(t) + \dot{\boldsymbol{h}}(t) + \boldsymbol{\omega}(t) \times (I(t)\boldsymbol{\omega}(t) + \boldsymbol{h}(t)) = T(t) \tag{17}$$

where $I(t)$ is the spacecraft inertia matrix, $\boldsymbol{h}(t)$ is the angular momentum of the spacecraft reaction wheels, and $T(t)$ is the external torque acting on the spacecraft. Inverting the inertia matrix and rearranging the terms, Eq. (17) becomes

$$\dot{\boldsymbol{\omega}}(t) = I^{-1}(t)([(I(t)\boldsymbol{\omega}(t) + \boldsymbol{h}(t))\times] - \dot{I}(t))\boldsymbol{\omega}(t) + I^{-1}(t)(T - \dot{\boldsymbol{h}}(t)) \tag{18}$$

Let $F(\boldsymbol{\omega}(t)) = I^{-1}(t)([(I(t)\boldsymbol{\omega}(t) + \boldsymbol{h}(t))\times] - \dot{I}(t))$ (note that this is not a unique representation[14]) and $\boldsymbol{u}(t) = I^{-1}(t)(T - \dot{\boldsymbol{h}}(t))$. Eq. (18) is then written as

$$\dot{\boldsymbol{\omega}}(t) = F(\boldsymbol{\omega}(t))\boldsymbol{\omega}(t) + \boldsymbol{u}(t) \tag{19}$$

In the pseudo-linear approach, Eq. (19) is treated as a 'linear' equation

$$\dot{\boldsymbol{\omega}}(t) = F(\hat{\boldsymbol{\omega}}(t))\boldsymbol{\omega}(t) + \boldsymbol{u}(t) \tag{20}$$

where $\hat{\boldsymbol{\omega}}(t)$ is the current estimate of the angular velocity. The angular velocity is propagated by discretely solving Eq. (20).

The external torques considered in Eq. (20) include an estimate of gravity gradient and the torque produced by the magnetic torque rods. The reaction wheel data is included, and the derivative of the reaction wheel momentum is computed numerically. The FUSE solar arrays reorient during a maneuver, thereby changing the spacecraft inertia. The derivative of the inertia matrix is computed numerically, based on the changing indexing angle of the solar arrays. The solar array inertia is converted to body coordinates with the array angle and added to the spacecraft body inertia.

HYBRID ALGORITHM

The hybrid algorithm used to estimate the FUSE attitude and rate is a combination of the pseudo-linear dynamics model with the IRP algorithm. The IRP algorithm is implemented as outlined above. First, the state is updated according to Eq. (12) with the magnetometer data. The covariance is updated according to Eq. (14). Next, the attitude matrix is computed with the updated state vector components and the a priori state vector components using Eq. (3). The state is then reset, and the attitude matrix is normalized using the following approximate orthogonalization method[12]

$$D^*(k+1|k+1) = (\frac{3}{2}\mathrm{I} - \frac{1}{2}D(k+1|k+1)D(k+1|k+1)^T)D(k+1|k+1) \tag{21}$$

The state is propagated with the acceleration model. The state transition matrix and the covariance matrix are first computed. The state and covariance are propagated with Eqs. (15) and (16), respectively. However, the angular rate is simultaneously propagated with the pseudo-linear equation given in Eq. (20), given discretely as

$$\hat{\boldsymbol{\omega}}(k+1|k) = \hat{\boldsymbol{\omega}}(k|k) + (F(\hat{\boldsymbol{\omega}}(k|k))\hat{\boldsymbol{\omega}}(k|k) + \boldsymbol{u}(k))\Delta t \tag{22}$$

where Δt is the propagation time interval and $\boldsymbol{u}(k) = I^{-1}(k)(T(k) - \frac{\boldsymbol{h}(k)-\boldsymbol{h}(k-1)}{\Delta t})$. Again, $T(k)$ is the sum of the estimated gravity gradient torque at time, k, and the magnetic torque. The reaction wheel momentum at time, k, is given by $\boldsymbol{h}(k)$. The term $\frac{\boldsymbol{h}(k)-\boldsymbol{h}(k-1)}{\Delta t}$ is the estimated derivative of the reaction wheel momentum.

At the end of the propagation cycle, the angular rate in the IRP estimated state vector is replaced with the rate propagated with the spacecraft dynamics.

$$\hat{\boldsymbol{x}}(k+1|k) = [\hat{\boldsymbol{\theta}}(k+1|k)^T\ \hat{\boldsymbol{\omega}}(k+1|k)^T\ \hat{\dot{\boldsymbol{\omega}}}(k+1|k)^T] \tag{23}$$

where $\hat{\boldsymbol{\omega}}(k+1|k)$ is given in Eq. (22). The process repeats as the IRP update cycle is performed with the hybrid propagated state vector.

This method resulted from an attempt to improve the FUSE attitude and rates estimated during a maneuver. Theoretical considerations on the impact of combining the two algorithms in a brute force manner are not given. Such a study is a subject for future research.

FUSE TEST RESULTS

The hybrid IRP-Euler filter algorithm is tested with several FUSE data sets. All the data sets contain maneuvers. In all of the cases with standard slew maneuvers, the IRP-Euler filter met the accuracy requirements. Examples from two data sets with typical slew maneuvers are presented first. The first data set contains two slew maneuvers. Figure 1 shows that the attitude estimate is within the two degree requirement, shown by a solid line at ± 2 degrees. Figure 2 shows that the rate estimate is within the 20 arc-sec/sec requirement, also shown as a solid line at ± 20 arc-sec/sec. Finally, Figure 3 shows the rate estimate, the dashed line, and the gyro data, solid line. The z axis is the noisiest, but is still within the requirements.

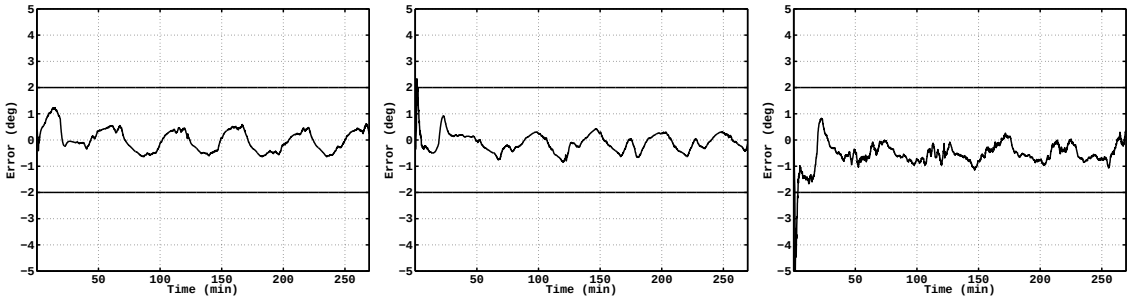

Figure 1 Attitude Errors for Day 68 of 2002 with 2 Degree Limit, (a) X Axis, (b) Y Axis (c) Z Axis

The second data set contains four maneuvers. The results are given in figures 4 through 6. Again, in all cases, the attitude and rate estimates are within the requirements.

Next, the combined algorithm is tested on data containing large maneuvers. First, results from a long, continuous maneuver are presented. Figure 7 shows that the attitude error requirements are met most of the time. The attitude errors on the Y axis exceed the 2 degree requirement 3 times, reaching approximately 3 degrees at one point, and the Z attitude errors reach -4 degrees at one point. Figure 8 shows also that the rate requirements are met, except during one portion of the maneuver on the Z axis. The rate errors on the Z axis reach -30 arcsec/sec at one point. Finally, Figure 9 shows that the rate estimate follows the gyro data during the maneuver.

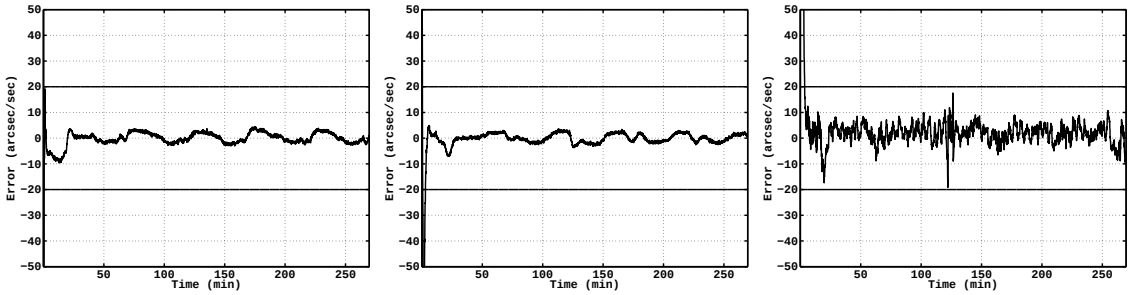

(a) (b) (c)

Figure 2 Rate Errors for Day 68 of 2002 with 20 arc-sec/sec Limit, (a) X Axis, (b) Y Axis (c) Z Axis

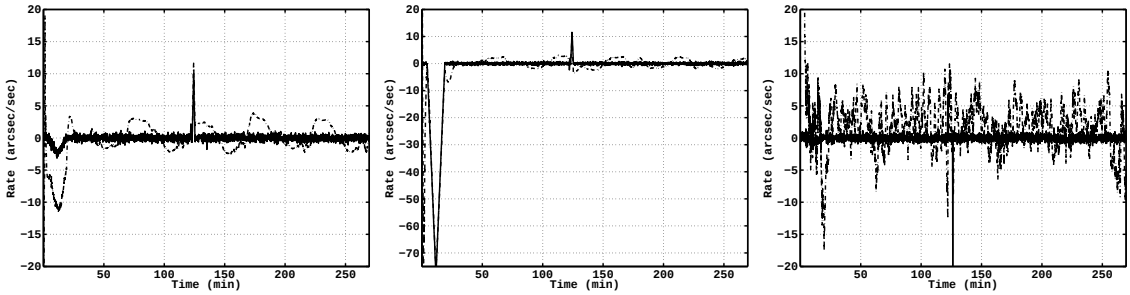

(a) (b) (c)

Figure 3 Estimated and Gyro Rates for Day 68 of 2002. Dashed line: Hybrid algorithm, solid line: gyro data, (a) X axis, (b) Y axis, (c) Z Axis

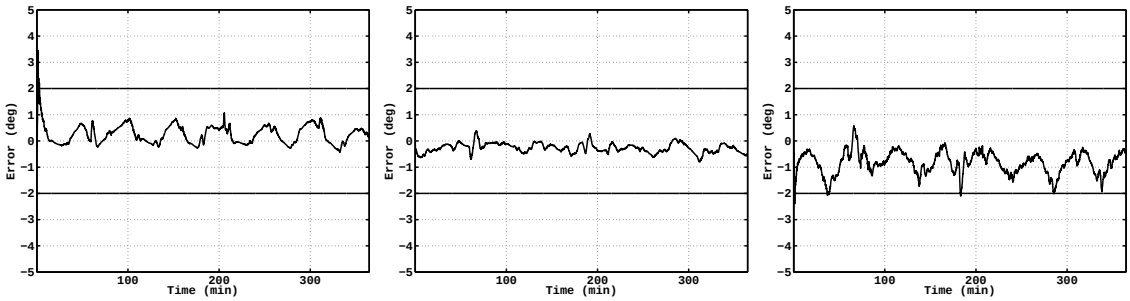

(a) (b) (c)

Figure 4 Attitude Errors for Day 80 of 2002 with 2 Degree Limit, (a) X Axis, (b) Y Axis (c) Z Axis

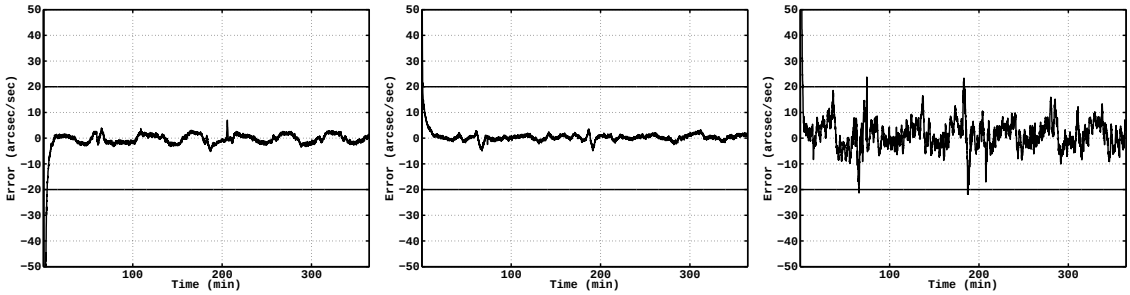

(a) (b) (c)

Figure 5 Rate Errors for Day 80 of 2002 with 20 arc-sec/sec Limit, (a) X Axis, (b) Y Axis (c) Z Axis

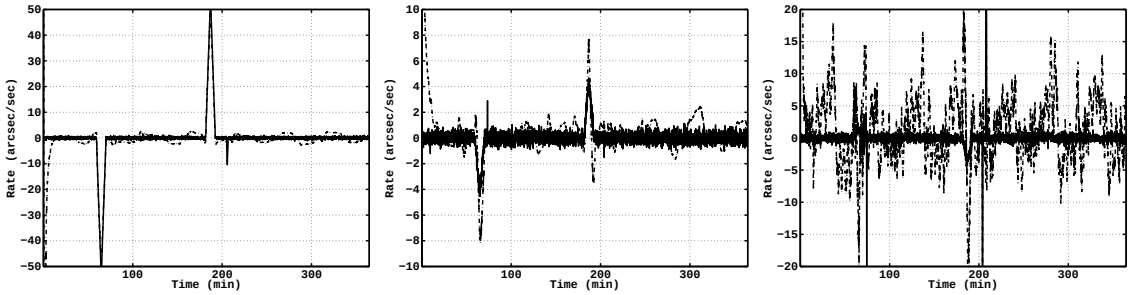

(a) (b) (c)

Figure 6 Estimated and Gyro Rates for Day 80 of 2002. Dashed line: Hybrid algorithm, solid line: gyro data, (a) X Axis, (b) Y Axis (c) Z Axis

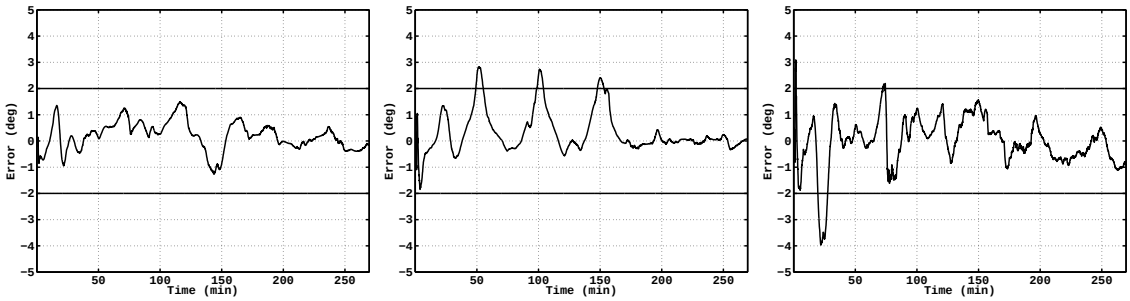

(a) (b) (c)

Figure 7 Attitude Errors for Day 102 of 2002 with 2 Degree Limit, (a) X Axis, (b) Y Axis (c) Z Axis

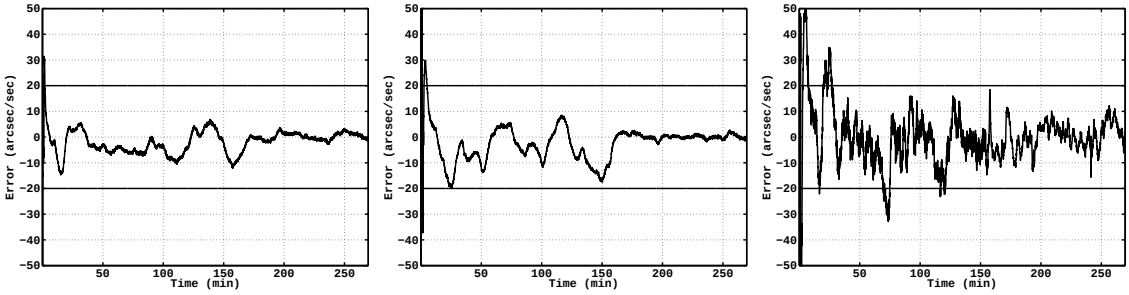

(a) (b) (c)

Figure 8 Rate Errors for Day 102 of 2002 with 20 arc-sec/sec Limit, (a) X Axis, (b) Y Axis (c) Z Axis

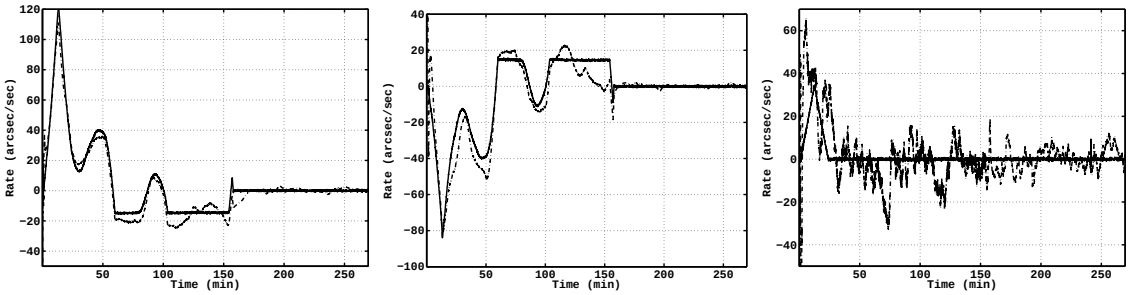

(a) (b) (c)

Figure 9 Estimated and Gyro Rates for Day 102 of 2002. Dashed line: Hybrid algorithm, solid line: gyro data, (a) X Axis, (b) Y Axis (c) Z Axis

The last data set presented contains a series of sequential maneuvers, desired to maneuver the spacecraft through a large angle. Figures 10 and 11 show that the attitude and rate requirements are met in the beginning, but fail near the end of the data, the attitude errors exceed 5 degrees in both the X and Z axes, and the rate errors exceed ± 50 arsec/sec. Figure 12 shows that the rate estimates follow the gyro data to some extent, but not as well as in previous data sets. The algorithm, as given, does not work well for this scenario.

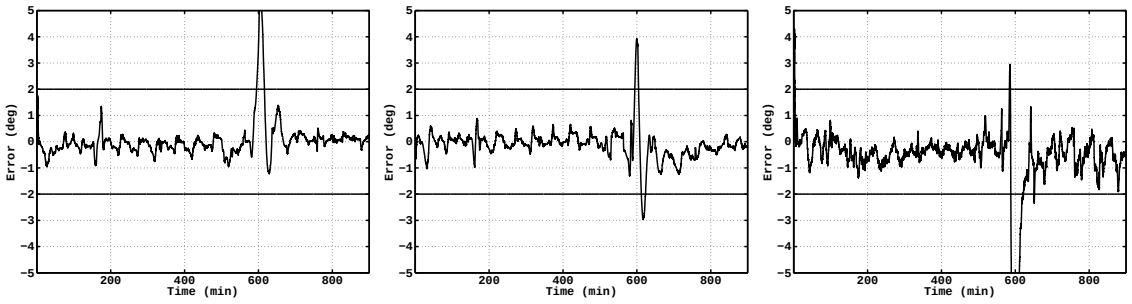

(a) (b) (c)

Figure 10 Attitude Errors for Day 99 of 2002 with 2 Degree Limit, (a) X Axis, (b) Y Axis (c) Z Axis

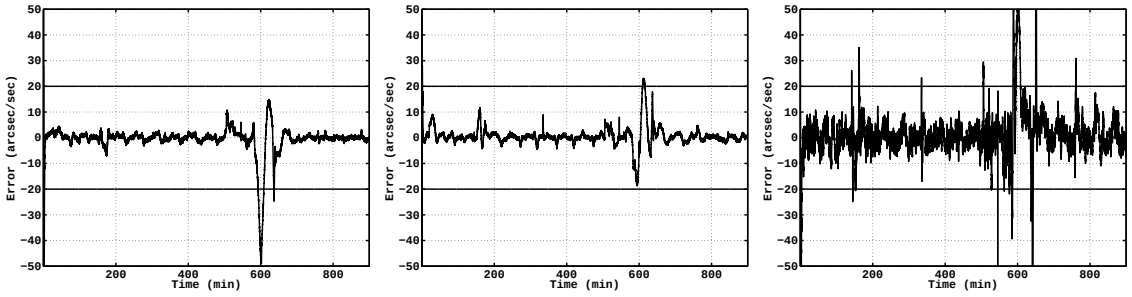

(a) (b) (c)

Figure 11 Rate Errors for Day 99 of 2002 with 20 arc-sec/sec Limit, (a) X Axis, (b) Y Axis (c) Z Axis

QUATERNION FEEDBACK CONTROL ALGORITHM

A simple closed loop simulation is developed to provide insight into the stability of the combined IRP-Euler algorithm with a feedback controller. The feedback control algorithm is a quaternion feedback control[15]

$$\boldsymbol{u}(t) = -k_p \tilde{\boldsymbol{\varepsilon}}_c(t) - k_D \boldsymbol{\omega}(t) \tag{24}$$

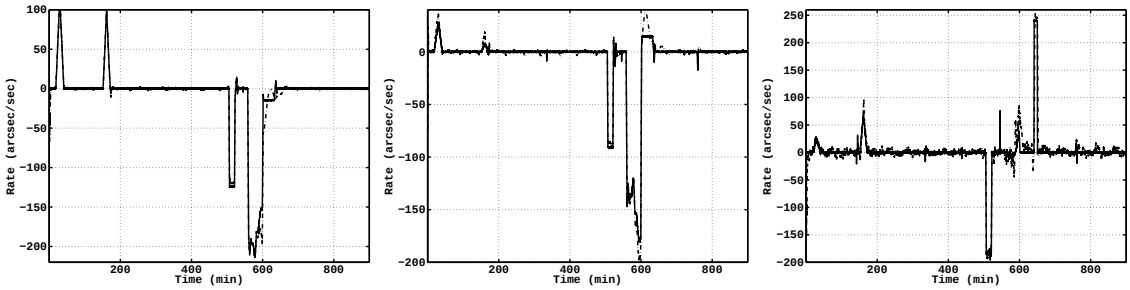

(a) (b) (c)

Figure 12 Estimated and Gyro Rates for Day 99 of 2002. Dashed line: Hybrid algorithm, solid line: gyro data, (a) X Axis, (b) Y Axis (c) Z Axis

where $\tilde{\boldsymbol{\varepsilon}}_c(t)$ is the vector part of the quaternion error, $\tilde{\boldsymbol{q}}_c(t) = [\tilde{\boldsymbol{\varepsilon}}_c(t)^T \, \tilde{\eta}_c(t)]$. The quaternion error is computed as

$$\tilde{\boldsymbol{q}}_c(t) = \boldsymbol{q}(t) \otimes \boldsymbol{q}_d^{-1}$$

where $\boldsymbol{q}_d$ is the desired quaternion, and is constant. Given perfect measurements, $\boldsymbol{q}(t)$ and $\boldsymbol{\omega}(t)$, the closed loop system, with the control given by Eq. 24, is globally, asymptotically stable.

The true quaternion and rate are not known. Instead, estimates of the quaternion and rate are provided by the IRP-Euler algorithm. In a certainty equivalence fashion, the estimates are used in Eq. 24 as

$$\hat{\boldsymbol{u}}(t) = -k_p \hat{\tilde{\boldsymbol{\varepsilon}}}_c(t) - k_D \hat{\boldsymbol{\omega}}(t) \tag{25}$$

The resulting closed loop system is asymptotically stable to within an RMS bound, given that the estimates are RMS bounded. The RMS error bounds of the closed loop system depend on the RMS bounds of the estimates, as well as the system parameters.

CLOSED LOOP SIMULATION TEST RESULTS

The initial closed loop simulation is intended to examine the stability properties of the closed loop system, comprised of the combined IRP-Euler algorithm and the quaternion feedback controller. The magnetometer measurements are corrupted with white noise. One reaction wheel along the spacecraft z axis is modeled, as well as three magnetic torque rods along each of the body axes (FUSE also has one operating skew wheel, but only the z axis wheel is included in this preliminary study for simplicity). The reaction wheel and torque rod data are not contaminated. The magnetometer data is not corrupted by the magnetic torque rods. The control $\hat{\boldsymbol{u}}(t)$ is resolved into a wheel torque and magnetic torque. The magnetic moment is limited to 130 Amp m^2 on each axis. The inertia matrix is a diagonal matrix, with the components [3550, 3390, 690] kg m^2 on the main diagonal.

The closed loop simulation run consisted of 1000 iterations, each iteration lasting approximately 60 minutes. The target quaternion direction is varied randomly in each iteration,

and the rotation angle is 20 degrees. Figure 13 shows the attitude error angles between the actual attitude and the target attitude at the end of 60 minutes for each of the 1000 iterations. In all cases, the errors are within 2 degrees. Figure 14 shows the errors between the true attitude and the estimated attitude at the end of 60 minutes for each iteration. Figure 15 shows the true rate, again at the end of 60 minutes for each iteration. In most cases, the rate is within 20 arc-sec/sec. Figure 16 is a single test case, showing the attitude error throughout a single iteration. Figure 17 shows the true rate during the maneuver, again throughout a single iteration.

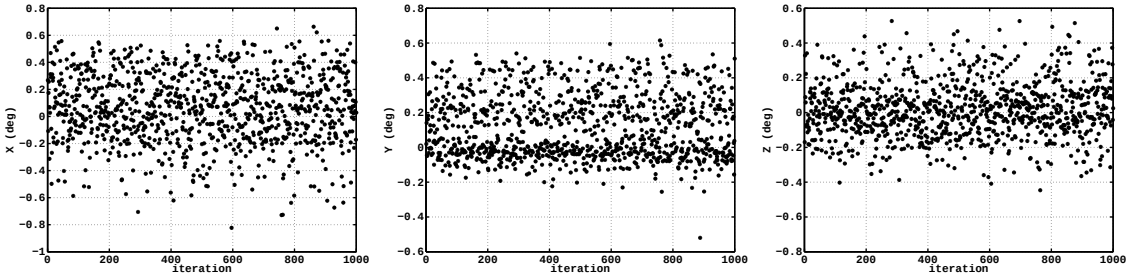

(a) (b) (c)

Figure 13 Actual Attitude Error Angles After 60 Minutes. (a) X Axis, (b) Y Axis, (c) Z Axis

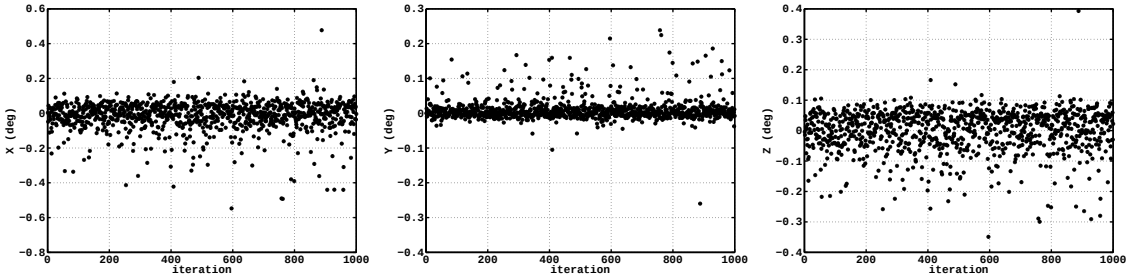

(a) (b) (c)

Figure 14 Attitude Estimation Error Angles After 60 Minutes. (a) X Axis, (b) Y Axis, (c) Z Axis

This preliminary simulation indicates that the closed-loop system is probably stable, given few disturbances. Additional simulations, with a more complex set of disturbances, is required. Examples of additional disturbances to be considered are gravity gradient torques, reaction wheel disturbances, reaction wheel control torque limits, magnetometer bias, and alignment errors.

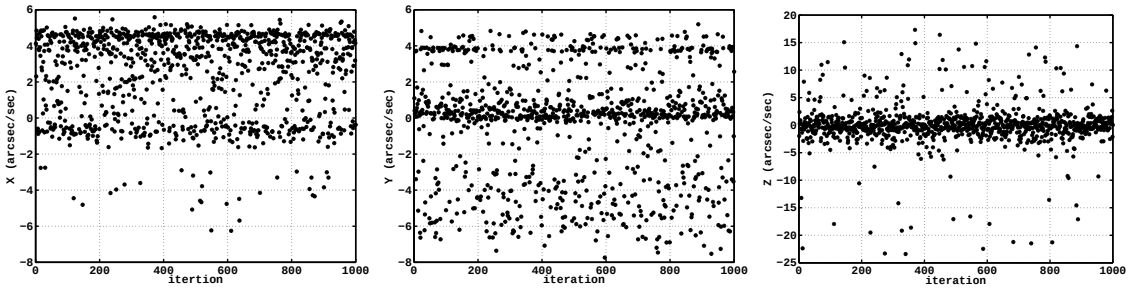

(a) (b) (c)

Figure 15 True Rates After 60 Minutes. (a) X Axis, (b) Y Axis, (c) Z Axis

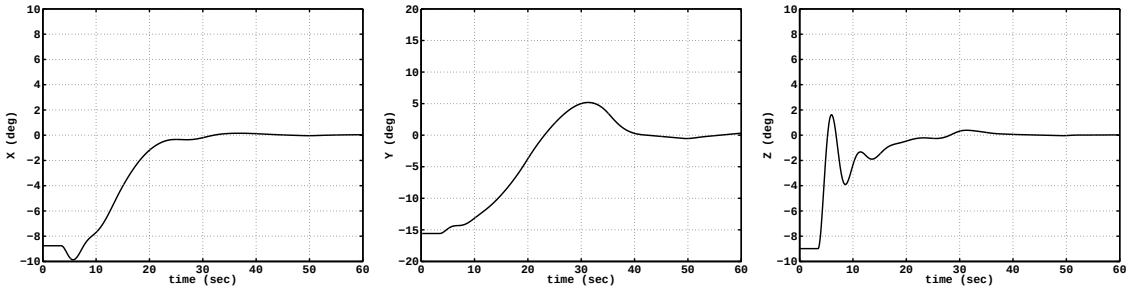

(a) (b) (c)

Figure 16 Actual Attitude Errors for 20 Degree Attitude Maneuver. (a) X Axis, (b) Y Axis, (c) Z Axis

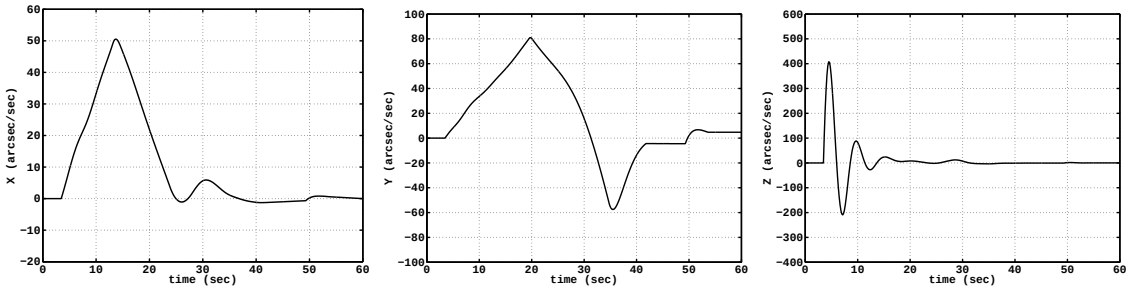

(a) (b) (c)

Figure 17 True Rates for 20 Degree Attitude Maneuver. (a) X Axis, (b) Y Axis, (c) Z Axis

CONCLUSIONS

Two estimation algorithms, designed to estimate spacecraft attitude and rate, are combined to provide the attitude and rate estimates for FUSE. The first algorithm, the IRP algorithm, uses a kinematic approach in modeling the angular acceleration of the spacecraft. The second algorithm, the pseudo-linear extended Kalman filter, relies on the spacecraft dynamics model in the rate propagation. The only attitude sensor available is a magnetometer. Combining the two algorithms into the hybrid IRP-Euler algorithm, provides attitude and rate estimates within the accuracy requirements for most maneuver scenarios. A preliminary closed loop analysis indicates that the IRP-Euler filter with a quaternion feedback control algorithm is stable for modest sized maneuvers. Additional work is required to determine the full range of stability for the closed loop system.

REFERENCES

1. "NASA's Hubble Project SM3A Web Site," URL: http://hubble.gsfc.nasa.gov/servicing-missions/sm3a.html [cited 25 July 2003].

2. Psiaki, M. L., Martel, F., and Pal, P. K., "Three Axis Attitude Determination via Kalman Filtering of Magnetometer Data," *Journal of Guidance, Control, and Dynamics*, Vol. 13, No. 3, 1990, pp. 506–514.

3. Challa, M. and Natanson, G., "Effects of Magnetometer Calibration and Maneuvers on Accuracies of Magnetometer-Only Attitude-and-Rate Determination," *AAS/GSFC International Symposium on Space Flight Dynamics*, AAS/GSFC, Greenbelt, Maryland, May 1998.

4. Azor, R., Bar-Itzhack, I. Y., and Harman, R. H., "Satellite Angular Rate Estimation from Vector Measurements," *Journal of Guidance, Control, and Dynamics*, Vol. 21, No. 3, 1998, pp. 450–457.

5. Harman, R. R. and Bar-Itzhack, I. Y., "Pseudolinear and State-Dependent Riccati Equation Filters for Angular Rate Estimation," *Journal of Guidance, Control, and Dynamics*, Vol. 22, No. 5, 1999, pp. 723–725.

6. Bar-Itzhack, I. Y., "Classification of Algorithms for Angular Velocity Estimation," *Journal of Guidance, Control, and Dynamics*, Vol. 24, No. 2, 2001, pp. 214–218.

7. Azor, R., Bar-Itzhack, I. Y., Deutschmann, J. K., and Harman, R. R., "Angular Rate Estimation Using Delayed Quaternion Measurements," *Journal of Guidance, Control, and Dynamics*, Vol. 24, No. 3, 2001, pp. 436–443.

8. Algrain, M. C. and Saniie, J., "Interlaced Kalman Filtering of 3-D Angular Motion Based on Euler's Nonlinear Equations," *IEEE Transactions on Aerospace and Electronic Systems*, Vol. 30, No. 1, 1994, pp. 175–185.

9. Oshman, Y. and Dellus, F., "Fast Estimation of Spacecraft Angular Velocity Using Sequential Measurements of a Single Directional Vector," *AIAA Journal of Spacecraft and Rockets*, Vol. 40, No. 2, Mar.–Apr. 2003, pp. 237–247.

10. Oshman, Y. and Dellus, F., "Fast Estimation of Spacecraft Angular Velocity from Sequential Geomagnetic Field Observations," *A Collection of the Technical Papers of the AIAA/AAS Astrodynamics Specialist Conference*, American Institute of Aeronautics and Astronautics, Reston, VA, 2000, pp. 322–330.

11. Oshman, Y. and Psiaki, M. L., "Spacecraft Attitude Rate Estimation From Geomagnetic Field Measurements," *Journal of Guidance, Control and Dynamics*, Vol. 26, No. 2, Mar.–Apr. 2003, pp. 244–252.

12. Oshman, Y. and Markley, L., "Sequential Attitude and Attitude-Rate Estimation Using Integrated-Rate Parameters," *Journal of Guidance, Control and Dynamics*, Vol. 22, No. 3, May–June 1999, pp. 385–394.

13. Oshman, Y. and Markley, F. L., "Spacecraft Attitude/Rate Estimation Using Vector-Aided GPS Observations," *IEEE Transactions on Aerospace and Electronic Systems*, Vol. 35, No. 3, July 1999, pp. 1019–1032.

14. Bar-Itzhack, I. Y., Harman, R. R., and Choukroun, D., "State-Dependent Pseudo-Linear Filters for Spacecraft Attitude and Rate Estimation," *AIAA Guidance, Navigation, and Control Conference*, AIAA, Monterey, California, August 2002.

15. Wie, B., *Space Vehicle Dynamics and Control*, AIAA Education Series, 1998.

16. Wertz, J. R., editor, *Spacecraft Attitude Determination and Control*, D. Reidel Publishing Company, 1984.